

Article

# Investigations on Material Loads during Grinding by Speckle Photography

Andreas Tausendfreund <sup>1,\*</sup>, Florian Borchers <sup>2</sup>, Ewald Kohls <sup>2</sup>, Sven Kuschel <sup>2,3</sup>,  
Dirk Stöbener <sup>1,3</sup>, Carsten Heinzel <sup>2,3</sup>  and Andreas Fischer <sup>1,3</sup> 

<sup>1</sup> Bremen Institute for Metrology, Automation and Quality Science (BIMAQ), University of Bremen, Linzer Straße 13, 28359 Bremen, Germany; std@bimaq.de (D.S.); andreas.fischer@bimaq.de (A.F.)

<sup>2</sup> Leibniz Institute for Materials Engineering IWT, Division Manufacturing Technologies, Badgasteiner Str. 3, 28359 Bremen, Germany; borchers@iwt-bremen.de (F.B.); kohls@iwt-bremen.de (E.K.); kuschel@iwt-bremen.de (S.K.); heinzel@iwt.uni-bremen.de (C.H.)

<sup>3</sup> MAPEX Center for Materials and Processes, University of Bremen, Bibliothekstraße 1, 28359 Bremen, Germany

\* Correspondence: a.tausendfreund@bimaq.de; Tel.: +49-421-218-64641

Received: 6 September 2018; Accepted: 12 October 2018; Published: 16 October 2018



**Abstract:** The knowledge of the loads occurring during a manufacturing process (e.g., grinding) and of the modifications remaining in the material is used in the concept of process signatures to optimize the manufacturing process and compare it with others (e.g., laser processing). The prerequisite for creating a process signature is that the loads can be characterized during the running process. Due to the rough process conditions, until now there is no in-process technique to measure the loads in the form of displacements and strains in the machined boundary zone. For this reason, the suitability of speckle photography is demonstrated for in-process measurements of material loads in a grinding process without cooling lubricant and the measurement results are compared with finite element method (FEM) simulations. As working hypothesis for the simulation it is assumed, that dry grinding is a purely thermally driven process. Despite the approximation by a purely thermal model with a constant heat source, the measured displacements differ only by a maximum of approximately 20% from the simulations. In particular, the strain measurements in feed speed direction are in good agreement with the simulation and support the thesis, that the dry grinding conditions used here lead to a primarily thermally affecting process.

**Keywords:** grinding; material load; speckle photography; FEM simulation

## 1. Introduction

Process-induced internal material loads directly cause workpiece modifications and generate the surface integrity of a workpiece (e.g., residual stress and hardness) [1]. The correlation between internal material loads and induced modifications is used in the concept of process signatures and can be used to design optimized processes and process chains specifically oriented on the functional properties of the final component [2,3]. For the prediction of residual stresses occurring in the grinding process, various theoretical approaches can be derived [4,5]. However, to gain comprehensive knowledge about the stresses acting during machining, it is necessary to characterize and analyze the loads while they are affecting the workpiece. Simulations can help to understand the effects of the elastic and plastic strains [6]. However, the simulations are usually simplified by approximations and do not always accurately reflect real conditions. Therefore, it is essential to determine the actual loads by in-process measurements and to validate the simulation results.

Although external loads such as forces affecting the workpiece during material processing can be measured and analyzed in detail (e.g., with force dynamometers), there is currently no in-process

measuring method that is capable of determining the strains in the contact zone. Steel integrated thin film sensors to measure the mechanical loads in test workpieces during the manufacturing process are subject of current scientific research [7–9]. However, this measurement approach is invasive and currently only allows single-point measurements with a limited spatial resolution in the millimeter range.

To enable non-invasive field measurements of displacement and strain with a high spatial resolution in the micrometer range, the digital speckle photography (DSP) is a promising measurement approach [10,11]. Theoretical considerations show that the fundamental uncertainty limits of speckle photography are only limited by Heisenberg's uncertainty relation [12]. For displacement measurements, uncertainties of less than 7 nm can be achieved with current camera and laser technology [12]. As a non-contact optical measuring method speckle photography is consequently predestined for fast and precise in-process measurements. Speckle photography was recently used for a rolling process [7] and a milling process [13], but has not yet been applied to investigate the grinding process.

For this reason, the aim is to demonstrate the usability of DSP for the in-process measurement of internal loads during grinding. The usage of cooling lubricant adds additional measurement challenges, because the movement of the cooling lubricant or the movement of containing particles, respectively, can be misinterpreted as material displacement. Therefore, the usability of the speckle measuring technology is tested in a first step in a dry grinding process without cooling lubricant. Furthermore, grinding parameters are chosen that tend to generate high thermal stresses and induce large displacements. Under these circumstances, however, strong sparks occur, which also move through the measuring field. The scientific question is, whether speckle photography measurements are possible despite the demanding in-process conditions and how to achieve robust image evaluation algorithms? Furthermore, finite element method simulations of the dry grinding process with the considered conditions are based on the assumption, that grinding is a purely thermally effected process [14,15], and the contact zone between the grinding wheel and the workpiece can be approximated as a constant heat source. However, the assumption could not be supported by real strain measurements yet, because up to now in-process measurements of displacements in the contact zone are not possible. For this reason, another research aspect of the article is whether the assumption of a constant heat source as contact zone is justified and valid for machining without cooling lubricant.

To answer the question about the usability of speckle photography and to validate the FEM simulations, the article is structured as follows: At first, the recorded material loads during grinding such as forces and powers are described in Section 2.1. Both are used as input variables for the numerical simulation, which is subsequently explained in Section 2.2. The theoretical background for the displacement and strain field measurements including the measurement principle of speckle photography then follows in Section 2.3. Section 2.4 shows the experimental setup for the speckle photography measurements during grinding. A comparison between the FEM simulations and the measurement results of the speckle photography are presented in Section 3. In the concluding Section 4, a summary of the comparison between speckle measurements and simulations and an outlook on future work is given.

## 2. Materials and Methods

### 2.1. Material Loads

Various methods allow in-process measurements of loads like forces, contact zone temperature and power during grinding [16–18]. These external loads cause internal loads of the workpiece-like stress, strain or internal heat distribution and their gradients which result in modification of the surface layer. For scientific purposes the forces are usually determined by piezoelectric-based force measurement systems [16]. In the present work, the tangential force  $F_t$  in direction of the cutting speed

$v_c$  are recorded with a three axis force measurement system. From the process parameters and force the specific grinding power  $P_c''$ ,

$$P_c'' = \frac{F_t \cdot v_c}{a_p \cdot l_g}, \tag{1}$$

as an indicator for the energy transformation is calculated where  $a_p$  describes the width of cut and  $l_g$  the contact length. This knowledge is used to calculate the heat flux  $\dot{q}$  into the workpiece as a fraction ( $0 \leq k_w \leq 1$ ) of the specific grinding power  $P_c''$  transferred to heat:

$$\dot{q} = k_w \cdot P_c'', \tag{2}$$

which is necessary for FE simulations to be compared with the measurements.

### 2.2. FEM Approach and Simulative Setup

For the comparison with the experimental measurements, finite element simulations are used to simulate the impact of the grinding process on the workpiece material. The material flow is considered in the used software *DEFORM-3D* from the company *Scientific Forming Technologies Corporation* (Columbus, OH, USA) by shifting the grid nodes. Since no coolant is applied in the experiments, it can be assumed that the thermal impact of the process is much higher than others like the mechanical, which is a common assumption in the analysis of grinding processes [14,15]. Therefore, the simulation setup is derived from Kuschel et al. [19], using a moving heat source on the workpiece surface. To represent the experimental setup more realistic, the simulative setup is transferred to a 3D elasto-plastic modelling approach. The geometrical boundary conditions which include the geometric contact length  $l_g$  and the tangential feed speed  $v_{ft}$ , which is referred to the heat source here, are applied from the grinding experiments. The heat flux is estimated as 60% of the specific grinding power according to Kuschel [19], which is an appropriate assumption for the dry grinding process. Heat transfer between the workpiece and the environment (air) is defined by a heat transfer coefficient of  $100 \text{ W}/(\text{mm}^2 \cdot \text{K})$ . Figure 1 shows a schematic view of the 3D model approach and the used boundary conditions.

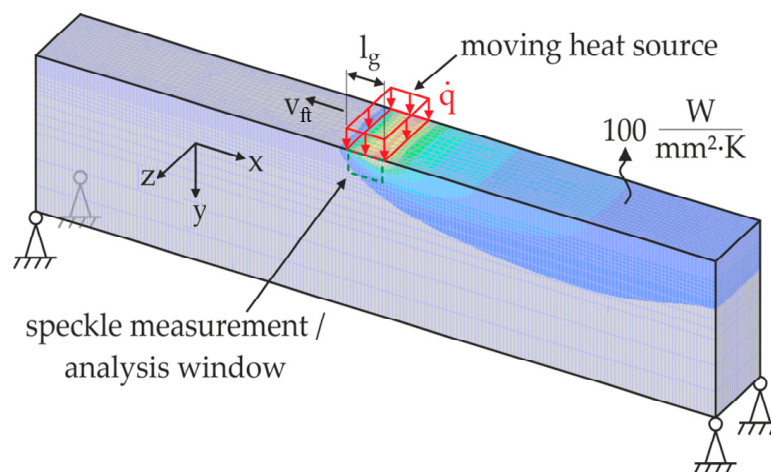


**Figure 1.** Schematic of the used model, boundary conditions, mesh and the temperature distribution (exemplary).

### 2.3. Displacement and Strain Field Measurement with DSP

Digital speckle photography is a well-known technique for characterizing in-plane displacements of surface elements [20,21]. A camera captures the coherent laser light, diffusely scattered at the surface. The phase elements of the light wave, modulated by the surface, generate an image of the topography in the image plane (on the camera chip), which is superimposed with a speckle pattern (Figure 2).

The size of the speckle can be varied in a wide range by the aperture of the lens. An outstanding feature of the subjective speckle is that they can be assigned to specific surface points, according to the imaging system. Therefore, shifts of individual speckle can be interpreted as displacements of local surface points in the object plane. A global displacement field of the measured surface is calculated by scanning a small evaluation window over the measurement field and calculating the cross correlation between two consecutive speckle images at each point. The size of the evaluation window can be computed automatically and should include at least three speckles on the diagonal. An optimal speckle diameter of about 3–5 pixels is adjusted [22]. By determining the shift of the correlation maxima, elastic and plastic deformations with previously unachieved spatial resolutions of about 20 nm and temporal resolutions in the microsecond range can be reconstructed [13]. After calculating the point displacement field  $\mathbf{P}(u, v)$  (where  $u$  and  $v$  are the displacements in the  $x$  and  $y$  directions), the deformation gradient field  $\mathbf{F}_{2D}$  can be determined according to Kajberg [23]:

$$\mathbf{F}_{2D} = \begin{pmatrix} 1 + \frac{\partial u}{\partial x} & \frac{\partial u}{\partial y} \\ \frac{\partial v}{\partial x} & 1 + \frac{\partial v}{\partial y} \end{pmatrix} \quad (3)$$

The polar decomposition of the  $\mathbf{F}_{2D}$  field leads to

$$\mathbf{F}_{2D} = \mathbf{R}_{2D}\mathbf{U}_{2D} \quad (4)$$

where  $\mathbf{R}_{2D}$  is the orthogonal rotation tensor ( $\mathbf{R}_{2D}^T\mathbf{R}_{2D} = \mathbf{I}$ ) and  $\mathbf{U}_{2D}$  is the positive definite and symmetric right stretch sensor ( $\mathbf{U}_{2D}^T = \mathbf{U}_{2D}$ ). Then  $\mathbf{F}_{2D}^T\mathbf{F}_{2D} = (\mathbf{R}_{2D}\mathbf{U}_{2D})^T\mathbf{R}_{2D}\mathbf{U}_{2D} = \mathbf{U}_{2D}^T\mathbf{U}_{2D}$ , which can be written in the form

$$\mathbf{U}_{2D}^2 = \mathbf{F}_{2D}^T\mathbf{F}_{2D} \quad (5)$$

To solve the square root, the spectral decomposition is used:

$$\mathbf{U}_{2D} = \lambda_1\mathbf{n}_1\mathbf{n}_1^T + \lambda_2\mathbf{n}_2\mathbf{n}_2^T \quad (6)$$

Here  $\lambda_1$  and  $\lambda_2$  are the square roots of the eigenvalues of the symmetric matrix  $\mathbf{U}_{2D}^2$  and  $\mathbf{n}_1$  and  $\mathbf{n}_2$  are the corresponding eigenvectors. The logarithmic (Hencky) in-plane strain matrix  $\boldsymbol{\varepsilon}_{2D}$  is finally computed as [24]

$$\boldsymbol{\varepsilon}_{2D} = \ln(\mathbf{U}_{2D}) \quad (7)$$

The basic setup for strain measurements in the surface grinding process is indicated in Figure 2. The measuring field is located on the side face—the unmachined side of the workpiece—directly at the border to the machined surface. The lens and the charged-coupled device (CCD) camera are fixed relative to the workpiece system, so that occurring speckle movements can be directly correlated with shifts of surface points. Out-of-plane deformations of the surface in the grinding process lead to a decorrelation of the speckle pattern, whereby the desired measuring effect is destroyed. The use of a high-speed camera (*Optronis: CP70*, Kehl, Germany) with a fast image-to-image evaluation at a frame rate of 167 fps, reduces this decorrelation since the out-of-plane displacement in the short period of 1/167 s is so small that almost no speckle decorrelation occurs. The measured displacements in the object plane are correspondingly small in this short time. However, with a suitable two-dimensional sub-pixel interpolation displacements of a few hundredths of a pixel (here 1 pixel  $\hat{=}$  1.94  $\mu\text{m}$ ) can be determined [25].

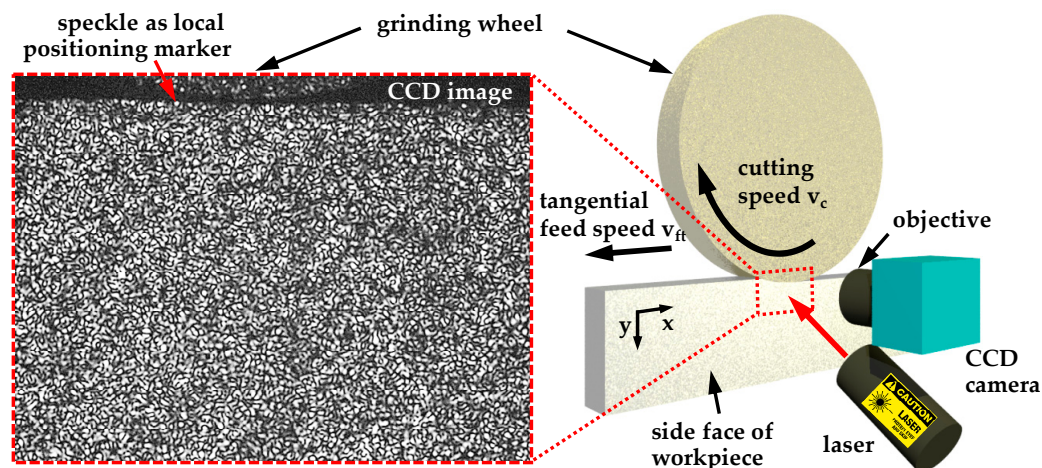


**Figure 2.** Measurement setup consisting of a laser and a CCD-camera and the captured image of the speckle pattern.

#### 2.4. Experimental Setup

The experiments are conducted on a *Blohm Profimat 412 HSG* (Hamburg, Germany) profile grinding machine with the process parameters to the displayed results shown in Figure 3. The presented parameters are one combination exemplarily selected from a variation of process parameter combinations. The parameters were selected to be in a practical range for a surface grinding process with consideration of the absence of cooling lubricants. Accordingly the estimated heat generation in the workpiece was considered. Integrated force and power measurements are used to record the external material loads. The applied abrasive tool is a vitrified bonded corundum grinding wheel with the specification 9A60H16. The material used in the experiments is alloy steel AISI4140 (42CrMo4) which is widely used in industrial applications. The selected heat treatment of the alloy steel leads to a normalized state, which is characterized by a ferrite-perlite microstructure. Thus, the surface hardness of the material is measured as 213 HV1 with a standard deviation of 3.6. The workpieces are designed as cuboids with a length of 165 mm, 18 mm width and 41.5 mm in height. To setup the peripherals (camera, laser and optical components) preferably close to the contact area, adapters and connection devices are constructed. The workpiece side-plane facing the speckle measuring system is shot-blasted before the experiments in order to generate a rough surface, which leads to a sufficient phase mixing of the laser wave front and to the formation of a fully developed and homogeneous speckle pattern. The measurement is performed on a spot in the middle section of the workpiece and the measurement setup is connected to the linear movement of the workpiece in x-axis direction. Therefore the tangential feed speed  $v_{ft}$  in this work is referring to the relative grinding wheel feed speed against the workpiece respectively the moving heat source. The feed of the workpiece is counter-directional to the cutting speed  $v_c$  of the grinding wheel (up-grinding) and thus the grinding wheel tangential feed speed  $v_{ft}$  is in the same direction as  $v_c$ .

The absence of the cooling lubricant in the investigated dry grinding process avoids measurement distortions due to irregular liquid and vapor behavior, creates a direct, clear optical channel for the camera and laser and protects the measuring system from contamination. However, the absence of the cooling lubricants leads to a strong development of flying sparks (see Figure 4). Optical components can be damaged by the red-hot chips and must be covered or placed at a correspondingly large distance from the point of the tool engagement. The large working distance of about 90 mm is achieved with a high-performance enlarging lens (*Rodenstock: Apo-Rodagon N*, Feldkichen, Germany).

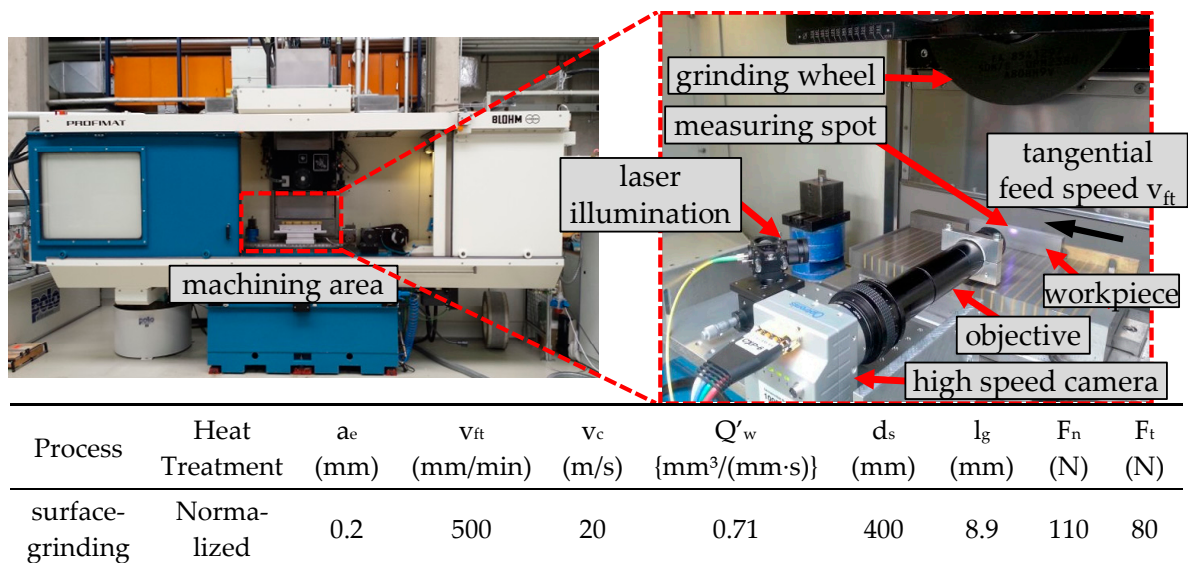


Figure 3. Blohm Profimat 412 HSG grinding machine and integrated measuring setup with process parameters.

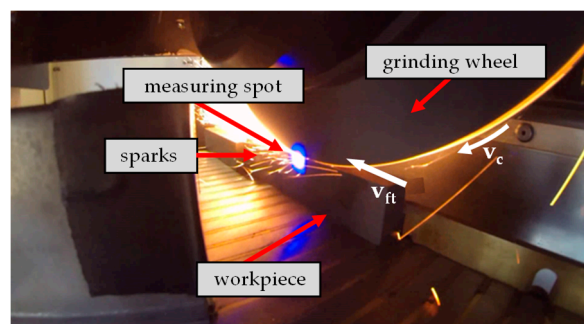


Figure 4. Surface grinding process with flying sparks.

The use of various extension tubes allows a threefold magnification, thus leading to a measuring field of about 6 mm × 8 mm. To stabilize the extension tubes and to ensure a fixed position of the CCD-camera in relation to the workpiece while grinding, a mounting fixture was designed. A fixation at the front end of the lens prevents the transmission of vibrations from the machine to the camera (see Figure 3). By adapting the camera system to the magnetic clamping plate which is setup on the force measurement plate, it is possible to take blur-free images of the object even during the grinding process. Thereby, vibrations are equalized for both measurement units and workpiece.

After grinding, a burr can be observed on the machined surface. The burr formation corresponds to a different inclination of the measuring surface, by what the light from the upper part of the workpiece area is not reflected into the camera. This leads to a loss of contrast of the speckle pattern at the upper edge of the workpiece and thus to a high measurement uncertainty in this region. Therefore, the displacement field of the contact zone near the surface is only calculated from a depth of approx. 800 μm below the machined surface, where the influence of contrast loss is reduced. Taking into account the depth of cut of  $a_e = 200 \mu\text{m}$ , the area between  $y = -1000 \mu\text{m}$  and  $y = 0 \mu\text{m}$  below the surface is not evaluated. Therefore, the boundary area is also not indicated in the simulation results.

In the dry grinding process the emergence of sparks and particles is misinterpreted by the conventional DSP analysis methods as displacement of surface points. The particle movement can be almost completely eliminated by using optimized algorithms. For this purpose, the size of the speckles inside the evaluation window is compared to the average speckle size in the global speckle image. Usually, disruptive particles caused by sparks are significantly larger than the adjusted speckle diameter and therefore immediately recognizable. In this case, the local deformation for the measuring

position is set to zero. The error that occurs while summing the displacements is negligible due to the high clock speed of the camera.

### 3. Results of In-Process Measurements and Simulations of Material Loads

In the following comparisons, the internal material loads in the workpiece surface during dry grinding are analyzed. For this purpose, the process is observed directly below the grinding wheel in the experiments. Respectively, the simulation results are determined while the constant heat source is right above the analysis window. To obtain an equally large, meaningful field of view for the measurement as for the simulation, the high amount of individual images of the measurement are stitched together to form a large field of  $6 \text{ mm} \times 32 \text{ mm}$ . Stitching is possible because the grinding wheel moves slowly through the measuring field at times  $t_1$  to  $t_{1+3n}$  during the image acquisition of the speckle pattern. Assuming a homogeneous workpiece and constant grinding conditions, each time step can be assigned to a certain grinding wheel position and thus, the global displacement field can be reconstructed (see Figure 5).

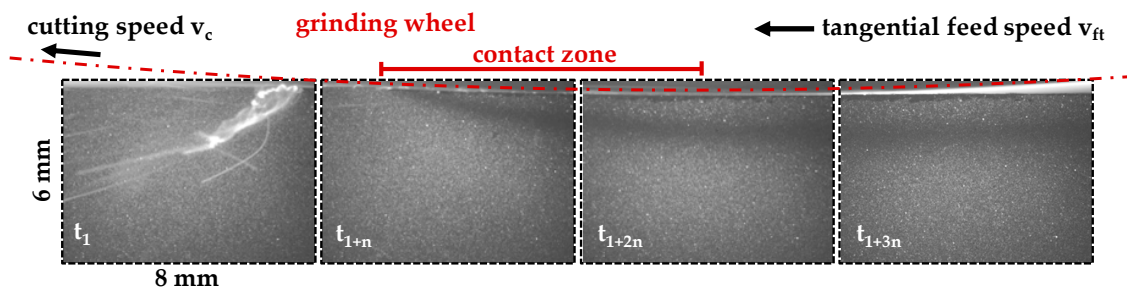
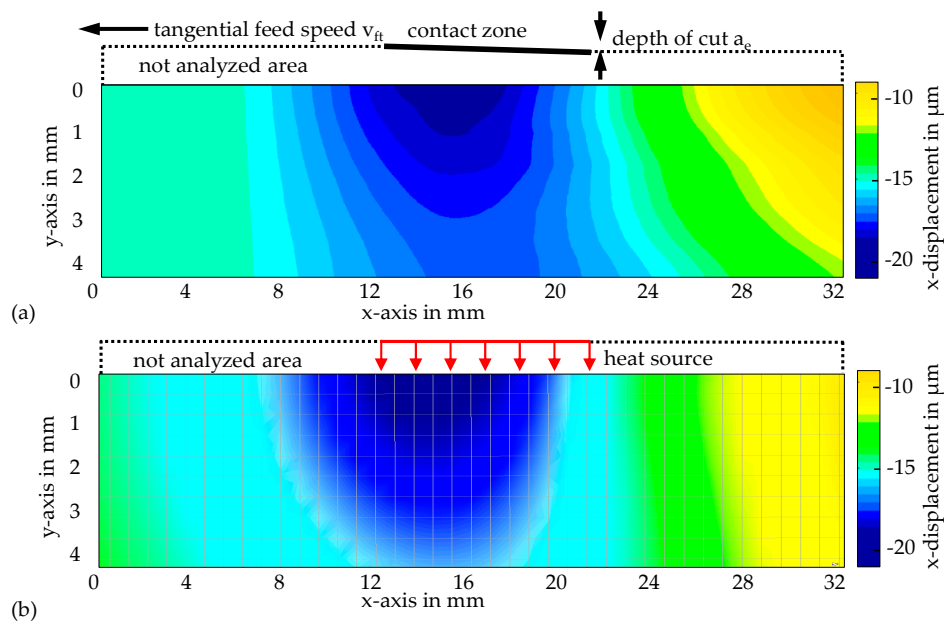


Figure 5. Sequence of individual speckle images, to reconstruct a large field of view of  $6 \text{ mm} \times 32 \text{ mm}$ .

The length of the contact zone (8.94 mm) is calculated from the grinding parameters (see Figure 3) and is in the dimension of a single speckle image. The partial image at time  $t_1$  shows an example of a picture with strong particle flight in the measuring field. The influence of the moving particles can be eliminated by a high recording rate and the special evaluation described in Section 2.4.

Despite the neglect of mechanical loads in the simulation, the simulation results show a qualitative accordance to the speckle measurements in feed speed direction ( $-x$ -displacements). In the simulation, however, the mechanical component caused by the force components described above is not considered. The tangential force component shifts the entire workpiece  $20 \mu\text{m}$  in the direction of the tool movement  $v_c$ . After subtraction of this offset, the values are in a good quantitative agreement. Figure 6 shows the total (elastic and plastic) displacements in feed speed direction, measured with the speckle photography (a) in comparison with the FEM simulations (b). The minimum displacement (=maximum negative displacement) lies in both cases approx. 2.5 mm after the first interaction between tool and workpiece and is  $22 \mu\text{m}$  in feed speed direction. Towards the end of the effective surface the displacement decreases to approx.  $-15 \mu\text{m}$ . The exact evaluation of the minimum displacement below the grinding wheel results in a value of 3 mm for the measurement and 2.2 mm for the simulation after the start of tool engagement. The discrepancy of  $800 \mu\text{m}$  is partly due to the fact that the beginning of the contact zone in the speckle images can only be defined optically (see subframe  $t_{1+n}$  in Figure 5), which is in principle subjective and can only be estimated. The relative measurement uncertainty resulting from the estimation for the position of the contact zone is approx.  $\pm 1 \text{ mm}$ . Within this framework, the positions of the  $x$ -displacement minimum in the measurement and in the simulation are congruent.



**Figure 6.** Total displacements during the process in feed speed direction: (a) measured with the speckle photography; (b) simulated.

The total displacements in normal direction are shown in Figure 7. The speckle measurements show a qualitatively similar behavior, but in the measurement the surface is shifted further down in the y-direction. In the measurement, the displacement 10 mm behind the heat source has increased to 25  $\mu\text{m}$ . In the simulation the calculated value of 20  $\mu\text{m}$  is 20% lower than in the measurements using speckle photography. This slight deviation may be caused by the neglect of the mechanical stress component in the simulation or by the fact that the assumed heat flow  $q_c$  over the contact length  $l_g$  cannot be regarded as constant or is higher than assumed.

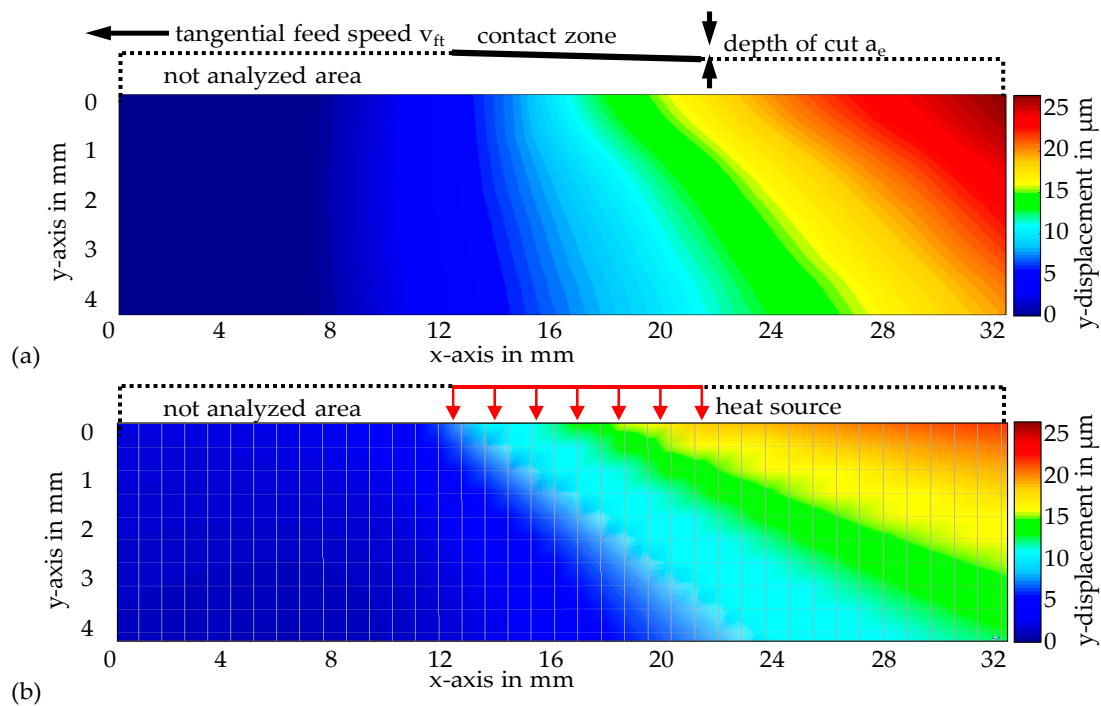


**Figure 7.** Total displacements during the process in normal direction: (a) measured with the speckle photography; (b) simulated.

The stepped behavior in the FEM simulation results from the limited number of nodes in the mesh of the large-volume 3D model (165 mm × 18 mm × 41.5 mm), which is discretized finer only at the interface to the heat source ( $y \rightarrow -1$  mm). As described in Section 2.2, the measured strain field has been calculated from the displacements determined by speckle photography. A good agreement can be seen for the resulting elongation during the grinding process in the feed speed direction (see Figure 8).

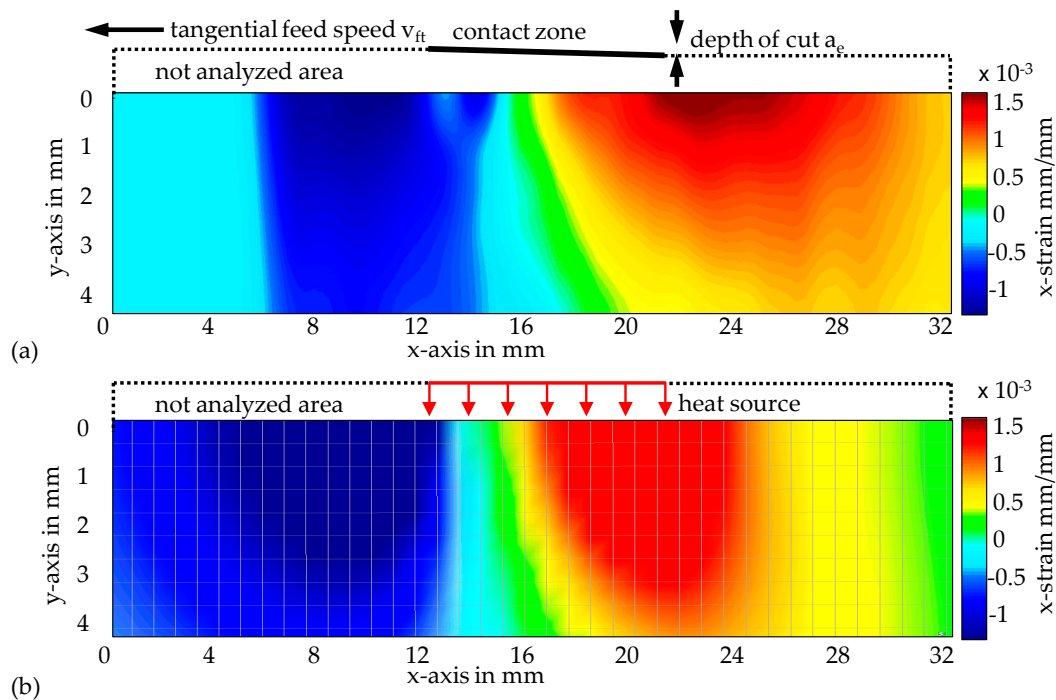


**Figure 8.** Total strain during the process in feed speed direction: (a) calculated from the speckle photography measurements; (b) simulated.

An interesting result is that the strain in front of the grinding wheel is obviously caused only by the thermal energy input and not by a mechanical effect. In the speckle measurement as in the FEM simulation, the minimum elongation lays approx. 3 mm in front of the grinding wheel and has a value of  $-1.2 \times 10^{-3}$  mm/mm. The maximum x-strain in the simulation is located at the end of the heat source. The peak value of  $1.3 \times 10^{-3}$  mm/mm is 15% lower than in the measurement, where it rises to  $1.5 \times 10^{-3}$  mm/mm. In the strain analysis as in the investigation of the displacements, a slight displacement of the measured data in the x-direction can be observed. The shifting between the measurement and the simulation is probably induced by an inaccurate visual determination of the contact zone in the speckle images.

Also for the strain in normal direction (see Figure 9) the simulation shows a slightly graduated behavior, caused by the limited possibilities of discretization and representation in the simulation tool *DEFORM-3D*. Nevertheless, the results for the simulation and the measurement for the y-strain are basically the same. No expansions build up in front of the grinding wheel or heat source respectively. Behind the influence zone, the strain values in both cases rise up to over  $2 \times 10^{-3}$  mm/mm.

Since the maximum values of the speckle measurement and the pure thermal FEM simulation for the displacement and strain analyses all in all differ only by a maximum of 20%, the simulation approach of a primarily thermally driven process for dry grinding can be regarded as valid.

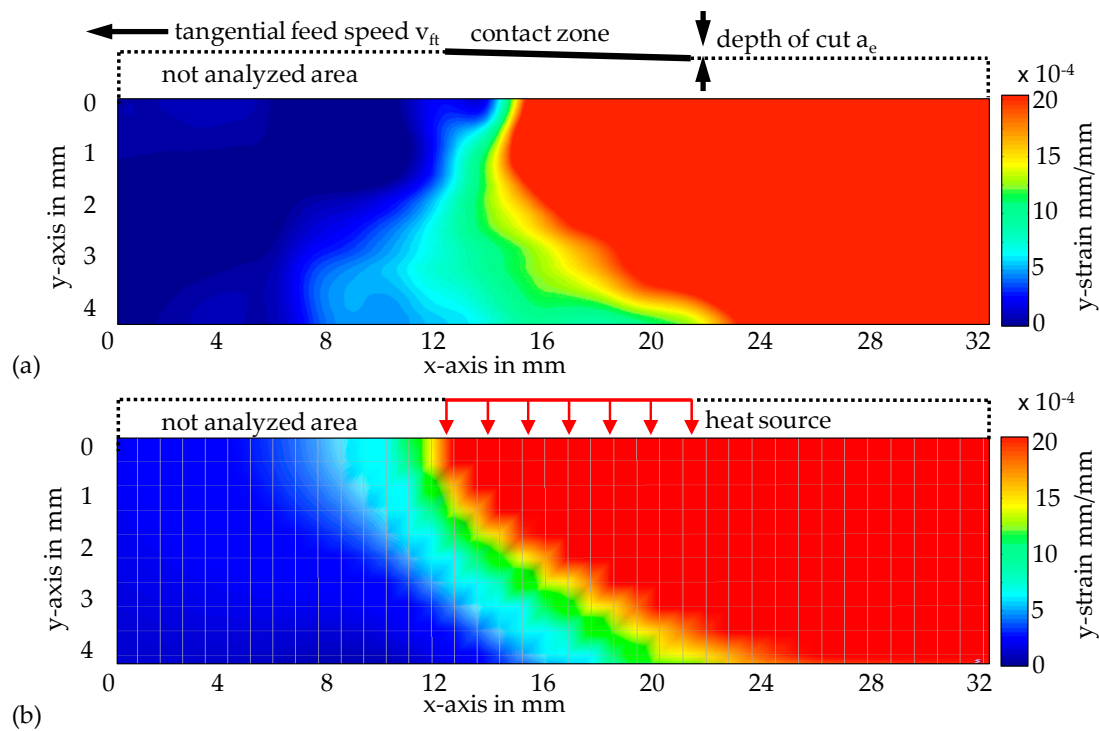


**Figure 9.** Total strain during the process in normal direction: (a) calculated from the speckle photography measurements; (b) simulated.

#### 4. Conclusions and Outlook

For the first time, process-accompanying displacement field and strain field measurements are carried out during a grinding process, in this case without application of cooling lubricant. Under these conditions, it can be assumed that the grinding process is predominantly thermally driven. Hence for the FEM simulation of this dry grinding process the model of a constant heat source was assumed. Despite this idealized assumption and the rough experimental conditions with flying sparks, the comparison between speckle photography measurement and FEM simulation shows a good agreement. Measurement and simulation indicate that the energy input takes place very locally. The negative strain that builds up in front of the grinding wheel is obviously primarily thermal in nature. The results demonstrate that speckle photography is able to measure strain fields during machining and confirm the assumption that thermal aspects prevail during the applied grinding process without coolant and therefore the process can be simulated by a constant heat source. In connection with the concept of process signatures, speckle photography shows that it can measure both elastic stresses and plastic changes in the material behind the tool. Thus, speckle photography is predestinated to acquire internal material stresses and to design optimized processes and process chains that are specifically oriented to the functional properties of the final component.

Future work will investigate whether the use of metalworking fluids is possible in the process and how they influence the measurements. First experiments have shown that speckle photography is possible through closed liquid films, where the air-liquid surfaces remain constant. Therefore, a measuring setup is currently being implemented with which the gap between workpiece and measuring system is completely filled with cooling lubricant. With an adapted grinding setup, the speckle photography also can be able to determine not only a dominant thermal but also a dominant mechanical impact of the loads.

**Author Contributions:** F.B., C.H. and E.K. designed the experiments. F.B. and E.K. performed the experiments. A.T., D.S. and A.F. elaborated the measurement technology and implementation. S.K. performed and evaluated the modelling and simulation. A.T., S.K., F.B. and E.K. analyzed the data. All authors participated in the elaboration and discussion of the manuscript.

**Funding:** This research was funded by the German Research Foundation (DFG) within the transregional Collaborative Research Center SFB/TRR 136 “Process Signatures” (in Bremen and Aachen (Germany) as well as Stillwater (OK, USA)) and in particular the subprojects F01, F06, C06 and M01.

**Conflicts of Interest:** The authors declare no conflict of interest. The founding sponsors had no role in the design of the study; in the collection, analyses, or interpretation of data; in the writing of the manuscript, and in the decision to publish the results.

## References

1. Jawahi, I.S.; Brinksmeier, E.; M'Saoubi, R.; Aspinwall, D.K.; Outiero, J.C.; Meyer, D.; Umbrello, D.; Jayal, A.D. Surface Integrity in Material Removal Processes: Recent Advances. *CIRP Ann. Manuf. Technol.* **2011**, *60*, 603–626. [[CrossRef](#)]
2. Brinksmeier, E.; Klocke, F.; Lucca, D.A.; Sölter, J.; Meyer, D. Process signatures—A new approach to solve the inverse surface integrity problem in machining processes. *Procedia CIRP* **2014**, *13*, 429–434. [[CrossRef](#)]
3. Kuschel, S.; Sölter, J.; Brinksmeier, E. Analysing internal material loads in manufacturing processes. *Adv. Mater. Res.* **2014**, *1018*, 83–90. [[CrossRef](#)]
4. Mahdi, M.; Zhang, L. Applied Mechanics in Grinding—V. Thermal Residual Stresses. *Int. J. Mach. Tools Manuf.* **1997**, *37*, 619–633. [[CrossRef](#)]
5. Walsh, D.G.; Torrance, A.A.; Tiberg, J. Analytical evaluation of thermally induced residual stresses in ground components. *J. Mech. Eng. Sci.* **2003**, *217*, 471–482. [[CrossRef](#)]
6. Liu, C.; Ding, W.; Yu, T.; Yang, C. Materials removal mechanism in high-speed grinding of particulate reinforced titanium matrix composites. *Precis. Eng.* **2018**, *51*, 68–77. [[CrossRef](#)]
7. Tausendfreund, A.; Stöbener, D.; Dumstorff, G.; Sarma, M.; Heinzl, C.; Lang, W.; Goch, G. Systems for locally resolved measurements of physical loads in manufacturing processes. *CIRP Ann. Manuf. Technol.* **2015**, *64*, 495–498. [[CrossRef](#)]
8. Dumstorff, G.; Sarma, M.; Reimers, M.; Kolkwitz, B.; Brinksmeier, E.; Heinzl, C.; Lang, W. Steel integrated thin film sensors for characterizing grinding processes. *Sens. Actuators A* **2016**, *242*, 203–209. [[CrossRef](#)]
9. Sarma, M.; Borchers, F.; Dumstorff, G.; Heinzl, C.; Lang, W. Measuring strain during a cylindrical grinding process using embedded sensors in a workpiece. *J. Sens. Syst.* **2017**, *6*, 331–340. [[CrossRef](#)]
10. Yamaguchi, I. Speckle displacement and decorrelation in the diffraction and image fields for small object deformation. *Opt. Acta* **1981**, *28*, 1359–1376. [[CrossRef](#)]
11. Goodman, J.W. *Speckle Phenomena in Optics. Theory and Applications*; Roberts and Company Publishers: Greenwood Village, CO, USA, 2007; ISBN 0-9747077-9-1.
12. Fischer, A. Fundamental uncertainty limit for speckle displacement measurements. *Appl. Opt.* **2017**, *56*, 7013–7019. [[CrossRef](#)] [[PubMed](#)]
13. Tausendfreund, A.; Stöbener, D.; Fischer, A. Precise In-Process Strain Measurements for the Investigation of Surface Modification Mechanisms. *J. Manuf. Mater. Process.* **2018**, *2*, 9. [[CrossRef](#)]
14. Outwater, J.O.; Shaw, M.C. Surface temperatures in grinding. *Trans. ASME* **1952**, *74*, 73–86.
15. Lavine, A.S. A simple model for convective cooling during the grinding process. *ASME J. Eng. Ind.* **1988**, *110*, 1–6. [[CrossRef](#)]
16. Martini, K.H. Multicomponent Dynamometers Using Quartz Crystals as Sensing Elements. *ISA Trans.* **1983**, *22*, 35–46.
17. Jermolajev, S.; Heinzl, C.; Brinksmeier, E. Experimental and analytical investigation of workpiece thermal load during external cylindrical grinding. *Procedia CIRP* **2015**, *31*, 465–470. [[CrossRef](#)]
18. Varghese, B.; Pathare, S.; Gao, R.; Guo, C.; Malkin, S. Development of a Sensor-Integrated “Intelligent” Grinding Wheel for In-Process Monitoring. *CIRP Ann. Manuf. Technol.* **2001**, *49*, 231–234. [[CrossRef](#)]
19. Kuschel, S.; Kolkwitz, B.; Sölter, J.; Brinksmeier, E.; Heinzl, C. Experimental and numerical analysis of residual stress change caused by thermal loads during grinding. *Procedia CIRP* **2016**, *45*, 51–54. [[CrossRef](#)]
20. Archold, E.; Burch, J.M.; Ennos, A.E. Recording of in-plane surface displacements by double-exposure speckle photography. *Opt. Acta* **1970**, *17*, 883–898. [[CrossRef](#)]
21. Stetson, K.A. A Review of Speckle Photography and Interferometry. *Opt. Eng.* **1975**, *14*, 482–489. [[CrossRef](#)]
22. Zhou, P.; Goodson, K.E. Subpixel displacement and deformation gradient measurement using digital image/speckle correlation (DISC). *Opt. Eng.* **2001**, *40*, 1613–1620. [[CrossRef](#)]

23. Kajberg, J.; Lindkvist, G. Characterisation of materials subjected to large strains by inverse modelling based on in-plane displacement fields. *Int. J. Solids Struct.* **2004**, *41*, 3439–3459. [[CrossRef](#)]
24. Eman, J.; Sundin, K.G.; Oldenburg, M. Spatially resolved observations of strain fields at necking and fracture of anisotropic hardened steel sheet material. *Int. J. Solids Struct.* **2009**, *46*, 2750–2756. [[CrossRef](#)]
25. Tausendfreund, A.; Stöbener, D.; Goch, G. Measuring technique for the detection of process force related component deformations in metalworking manufacturing processes. In Proceedings of the 5th International Conference on Distortion Engineering (IDE), Bremen, Germany, 23–25 September 2015; pp. 355–364.



© 2018 by the authors. Licensee MDPI, Basel, Switzerland. This article is an open access article distributed under the terms and conditions of the Creative Commons Attribution (CC BY) license (<http://creativecommons.org/licenses/by/4.0/>).